Aquaphotomics for monitoring of groundwater using short-wavelength near-infrared spectroscopy

Kovacs, Zoltan ; Muncan, Jelena ; Veleva, Petya ; Oshima, Mitsue ; Shigeoka, Shogo ; Tsenkova, Roumiana

(Citation)
Spectrochimica Acta Part A: Molecular and Biomolecular Spectroscopy,279:121378

(Issue Date)
2022-10-15

(Resource Type)
journal article

(Version)
Version of Record

(URL)
https://hdl.handle.net/20.500.14094/90009342

Spectrochimica Acta Part A: Molecular and Biomolecular Spectroscopy 279 (2022) 121378

Contents lists available at ScienceDirect

Spectrochimica Acta Part A: Molecular and Biomolecular Spectroscopy

journal homepage: www.elsevier.com/locate/saa

Aquaphotomics for monitoring of groundwater using short-wavelength near-infrared spectroscopy

Zoltan Kovacs [a,1], Jelena Muncan [b,1], Petya Veleva [c], Mitsue Oshima [d,e], Shogo Shigeoka [d,e], Roumiana Tsenkova [b,*]

[a] Department of Measurements and Process Control, Institute of Food Science and Technology, Hungarian University of Agriculture and Life Sciences, 14-16 Somlói str, Budapest 1118, Hungary
[b] Aquaphotomics Research Department, Graduate School of Agricultural Science, Kobe University, 1-1, Rokkodai, Nada, Kobe 657-8501, Japan
[c] Trakia University, Department of Agricultural Engineering, Agricultural Faculty, Stara Zagora 6000, Bulgaria
[d] Shigeoka Co. Ltd, 898 Konono, Hashimoto City, Wakayama 648-0086, Japan
[e] Yunosato Aquaphotomics Lab, 1075 Konono, Hashimoto City, Wakayama 648-0086, Japan

HIGHLIGHTS

- Impact of environmental temperature and humidity on SW-NIR water spectra examined.
- Environmentally-stable water matrix coordinates (WAMACS) identified.
- Ground water spectral pattern used for screening of water during 3 years.
- Aquaphotomics offers reagent-free, continuous, nondestructive water monitoring.

GRAPHICAL ABSTRACT

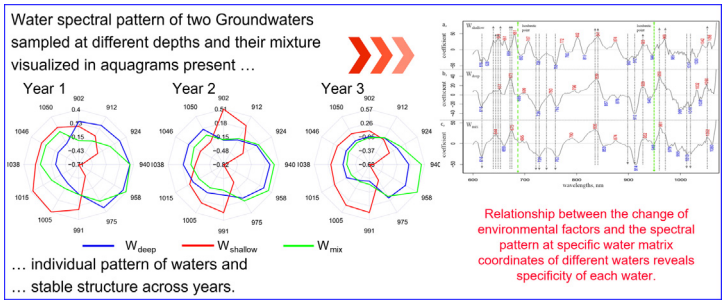

ARTICLE INFO

Article history:
Received 19 January 2022
Received in revised form 22 April 2022
Accepted 9 May 2022
Available online 11 May 2022

Keywords:
Aquaphotomics
Spectral monitoring
Water molecular system
Water quality
Environmental factors

ABSTRACT

Water spectrum of any aqueous system contains information about OH covalent and hydrogen bonds that are highly influenced by the environment and the rest of the molecules in the system. When aquaphotomics is used to analyze the water near infrared (NIR) spectra, the information about the water molecular structure can be obtained as a function of internal and external factors.

The objective of this research is to apply aquaphotomics analysis to evaluate different groundwaters by using their NIR unique spectral pattern, robust to external influences of temperature and humidity, that can potentially be used for water type identification and screening practice. Two groundwaters obtained at different depths and their mixture, differing in mineral content and molecular structure were monitored on a daily basis using portable visible/NIR (vis/NIR) spectrometer during three consecutive years. The spectra were pre-processed by smoothing and multiplicative scatter correction (MSC) to remove noise and baseline effects. Results showed that NIR spectral patterns of groundwater samples were affected by changes in environmental factors – temperature, humidity, time and others. The water absorbance bands which are highly influenced by humidity and temperature in short wavelength NIR region were identified. Their avoidance resulted in obtaining consistent spectral patterns during the entire monitoring period, unique for each groundwater, that can be used as its fingerprint and monitored over time.

* Corresponding author.
E-mail addresses: kovacs.zoltan.food@uni-mate.hu (Z. Kovacs), jmuncan@people.kobe-u.ac.jp (J. Muncan), m.oshima@spa-yunosato.com (M. Oshima), s.shigeoka@spa-yunosato.com (S. Shigeoka), rtsen@kobe-u.ac.jp (R. Tsenkova).
[1] Both authors contributed equally to writing of the manuscript.

https://doi.org/10.1016/j.saa.2022.121378

Consistency and uniqueness of the spectral pattern for each groundwater provide a potential to use the deviation of spectral pattern as an indicator of changes in the water. These results confirm that vis/NIR spectral pattern can be used as an integrative marker of water status, stable over time, providing the basis for an efficient cost-effective method for monitoring of water functionality.

1. Introduction

Understanding the water as a complex molecular system is of paramount importance due to its exceptional role in living organisms and the biological world in general. Despite being an essential requirement for a living world, the contemporary science and technology are still far from understanding many of the intricacies of the water molecular structure, its properties and functionality. Many research studies have been devoted to investigation of water from the chemical [1], physical [2], medical [3], agricultural [4] and other aspects. Immense number of publications deals with the topic of water quality [5-10]. The significance of water as a medium in which all biochemical reactions that sustain life are being carried out is most probably due to its molecular structure flexibility and highly reactive nature. Liquid water can be described as a complex, dynamic molecular network that changes its molecular structure and functionality easily owing to the strong potential for hydrogen bonding, highly sensitive to any perturbation [11-13]. Despite numerous techniques being applied for water characterization and better understanding of its structure – functionality relationship, its many aspects are still poorly understood and real-time monitoring methods of water molecular structure are still not available.

Visible/Near Infrared (vis/NIR) spectroscopy uses the visible and near-infrared region (400–2500 nm) of the electromagnetic spectrum to measure various physical and chemical parameters of the samples of interest [14]. It is a rapid, non-destructive and highly accurate analytical technique developed with the purpose of qualitative and quantitative evaluation of numerous and versatile products [15].

Aquaphotomics has been introduced as a novel approach [13] in the field of vis/NIR spectroscopy, which utilizes the water absorbance spectral features for a characterization of the samples, in an indirect way collecting the information about the chemical composition and environmental conditions as if the water is a "collective mirror" providing the information about the relationship between the water spectral pattern of the sample and its functionality.

Water spectrum contains information about covalent OH and hydrogen bonds highly influenced by the rest of the molecules in the solution and the environmental factors. As water is unique among small molecules, forming the tetrahedral but flexible, highly dynamic, hydrogen bond network, on a molecular level it can be considered as a sensor – responsive to any changes within/without [12,16]. When it comes to the interaction with other molecules present, the water on a molecular level could be considered as an amplifier, since, due to the small size and the hydrogen bonding of water molecules, the influence of just one alien molecule will always affect many water molecules [12,16]. The spectrum of water (or any aqueous or biological system) therefore, will represent a highly responsive signal, reflecting the water molecular structure and its changes, amplifying the effects of minute concentrations in solution and capturing changes in the environment. Utilization of water spectral features in vis/NIR region, enables aquaphotomics high sensitivity of detection for even traces of analytes, and even when analytes themselves do not absorb light in this region [13,17-21]. The advantages of this method have been so far used in a large variety of applications from basic molecular studies [18,22-29] to complex applications in food and agricultural sector [30-37], microbiology [38-41], diagnostics and monitoring [42–46,47], material and colloid science [48-51], environmental control and others [12].

One of the most direct applications is naturally in water quality monitoring. There are several previous studies, utilizing different parts of water NIR spectra, namely 1st overtone (around 1450 nm), 2nd and 3rd (located around 970 nm and 740 nm, respectively) to demonstrate the feasibility of the approach for water quality monitoring in different settings, such as in household purification systems [51], directly at the groundwater source [52], as a part of control of commercial mineral water products [53], control of environmental water pollution [54] and other systems [55]. These studies repeatedly evidenced that the spectral pattern of water can be used as its distinctive marker, an identifying signature for each sample, which integrates all the information about the composition of the samples in the particular environment, at particular time point. Then, the quality of water can be expressed as a certain set of states – defined by the composition and influence of environment, within some boundary values – i.e. limits, that, if crossed, can present a clear signal that the state of water is outside the "quality limits"; that something unusual happened either in the chemical content or in the environment. In order to make it more specific, a good strategy would be to define a spectral pattern using absorbance bands of water that are not easily influenced by some common changes in the environment that can mask the actual loss of desired quality.

The absorbance bands of water originate from different water molecular structures, such as free water molecules, dimers, trimers, protonated clusters and other [13]. The absorbance at these bands is not only changed in response to compositional changes in water, but also when the environmental parameters, such as temperature, pressure, humidity change. The effects of temperature on water spectra have been a research topic for a long time, but most of the research was performed using infrared region or the NIR region of first overtone of water located around 1450 nm [56-63]. Rare are the studies that examine the influence of fluctuations in pressure, humidity or temperature of the normal ambient on properties and structure of drinking water [63]. However, the temperature and relative humidity have large influence on water properties, such as evaporation rate, solvation ability, compressibility, heat capacity and others [64] and while those properties are not usually considered as "quality parameters", they are a matter of importance for the functionality of water and highly influence the water spectrum.

From another aspect, the 2nd and 3rd overtone of water are studied even less, although they are located in the region where NIR light has higher energy and provides longer penetration depth, which makes it especially useful for the development of portable instruments that can be used in any environmental setting. How the water absorbance changes at specific bands in response to the temperature and humidity of the environment is not researched well, but existing studies [64,65] point out to the importance of recognizing it, since it can have profound influence on the measured spectra and the accuracy of quantitative analyses. The effect of different environmental parameters such as tempera-

ture perturbation or humidity on the water near infrared spectra has been studied by many researchers [57,66,67]. However, it has not been studied how the different environmental factors over the years affect the spectral pattern of groundwater samples having different composition in the spectral range of the second and third overtone of OH, region of interest for development of portable instruments.

Considering the introduced problems, and building on the previous experiences [51,52], the focus of aquaphotomics application in this work was placed on achieving the following objectives:

- Identify the effects of environmental temperature and relative humidity on the spectral pattern of groundwaters in the short wavelength NIR region (2nd and 3rd overtone of water), in the terms of which water absorbance bands are most sensitive to these perturbations
- Define specific water spectral pattern for each of the investigated groundwaters in the short wavelength NIR region (2nd and 3rd overtone of water), that is stable against the environmental influences of temperature and humidity and can be used for their evaluation, comparison and quality monitoring.

2. Materials and methods

2.1. Samples

Groundwater samples from the Sambagawa Belt in Konono, Wakayama Prefecture, Japan (34°18′ N, 135°34′E) at two different depths about 50 m ($W_{shallow}$) and 1180 m (W_{deep}) were used as a study material. The third sample was regularly prepared as a mixture (blend) W_{mix} of 10 %W_{deep} and 90 %$W_{shallow}$. The physicochemical properties were analyzed during this study at the Kyoto City Industrial Technology Research Institute, Kyoto, Japan (Table 1). As W_{deep} water is from a deeper source it has higher mineral content and higher electrical conductivity, while the opposite is the case with $W_{shallow}$ as described in Table 1.

2.2. Near infrared spectroscopy

Visible and near-infrared (vis-NIR) spectral acquisition of the water samples had been performed daily during the period of three consecutive years, with a portable instrument FQA NIR-GUN (FANTEC Research Institute, Japan) in transflectance mode to yield absorbance values, using a 10 mm open-top liquid cuvette. Both the spectrophotometer and the water samples were kept in the same room for half an hour prior to the spectral acquisition to make sure they are equilibrated to the same environment. After placing the sample in the cuvette, three consecutive spectra were recorded over the entire spectral region (588 – 1092 nm), with 2 nm step. The physical parameters of the water samples and the environment such as temperature, humidity, and atmospheric pressure have been recorded at the time of measurement, as well as other information that could be of interest such as who performed the measurements, time and date of measurements, the state of the instrument, and similar.

2.3. Data analysis

Descriptive univariate statistical calculations were performed using the Box-and-Whisker plot [68] method to analyze the recorded physical parameters of the water samples and the environment.

The noisy parts of the recorded absorbance spectra was truncated and the spectral range between 600 and 1060 nm was preprocessed using Savitzky-Golay smoothing [69] with 2nd order polynomial filter with 11 points, followed by multiplicative scatter correction (MSC) [69] to remove the possible baseline fluctuations. Principal component analysis (PCA) [70] was used to describe multidimensional patterns of the NIR spectral dataset and to discover outliers.

Partial least squares regression (PLSR) was used as a quantitative analysis [69] of the preprocessed absorbance spectra to model and explore the relationship between the water structural changes and the physical parameters measured by reference methods. Each model was tested using cross-validation, where a part of the sample set was excluded from the calibration set, and the generated model was validated on the excluded samples (validation set). The procedure was repeated iteratively to ensure that all the samples were included in the validation set once. During this data splitting, as a principle, the consecutive scans of the individual samples were introduced all together either in calibration or in validation set to avoid the too optimistic validation. The cross-validation was performed by leave-one-temperature level-out and leave-one-humidity level-out for the modelling of temperature and humidity, respectively. This means that all the water spectra which were recorded at the same temperature (for instance at 26.0 °C) were used as a test set, while the model was built using all the spectra recorded at different temperatures and this splitting was iteratively repeated until each temperature level was used as test set. In a similar way calibration and validation were performed for modelling humidity.

Precision and accuracy of the quantitative PLSR models were evaluated by the following statistics: the coefficient of determination (R^2), root mean squared error (RMSE), and residual prediction deviation (RPD) which indicates the ratio of RMSE to standard deviation of reference values (SDY) [71]. The respective statistics were calculated for calibration and cross-validation. In order to avoid overfitting, maximum number of latent variables was determined as a 1/10th of total number of observations in models according to the recommendations [72].

In order to identify which water absorbance bands are particularly influenced by the changes in temperature and humidity of the environment, the regression vectors of PLSR models were inspected to find the common trend in absorbance behavior with respect to temperature and humidity respectively, in PLSR models for each water. This was performed in a following way. First, the highest peaks (positive and negative) in the regression vectors of PLSR temperature models made for each of the waters were identified. The position of these peaks reveals the position of absorbance bands at which there was a highest correlation between the absorbance of water and measured temperature. Following this, for each peak identified in either of the 3 regression vectors, the remaining two regression vectors were inspected to check if

Table 1
Selected physical and chemical properties of groundwaters examined in this study.

Water	Electrical conductivity (μS/cm)	Ion content (mg/L)				
		Ca	Mg	Na	Cl^-	SO_4^{2-}
W_{deep}	1700	180	57.8	165	212.578	0.248
$W_{shallow}$	357	29.5	7.69	37.6	24.164	0.014

there is a peak at the same location, or if there was not, if the sign of the regression coefficient at this particular position is the same. If there was the peak at the same place, or if the sign was the same, the "common" i.e. the same trend of absorbance behavior in respect to the change in temperature/humidity was assumed for all three waters. The common peaks for all three waters were then summarized according to their location and sign, and their tentative assignment based on the current literature sources was interpreted.

The absorbance values at specific water matrix coordinates (WAMACs) [13] define the water spectral pattern (WASP) which can be graphically represented by a chart called aquagram [73,74]. The aquagram displays the MSC transformed, normalized and averaged absorbance values of different sample groups at selected water absorbance bands.

In order to find which wavelengths can be used as WAMACs for the description of the state and dynamics of an aqueous system, the usual practice is to perform an array of analyses like principal component analysis, partial least squares regression using different dependent variables, discriminating or classification analysis, calculation of difference spectra (by subtracting the mean spectrum, the spectrum of pure water etc.), a practice described in a protocol of aquaphotomics analysis [74]. The goal of all these analyses is to find the consistently repeating absorbance bands among the most influential variables in the numerical outputs of the analyses such as loading vectors, discriminating powers, regression coefficient vectors, difference spectra. Following the procedure for finding the WAMACs as described for the 1st overtone of water [74], the WAMACs specific for description of a particular aqueous system can be found for any chosen spectral region, as the previous research studies have done for 2nd and 3rd overtone of water [52]. The particular steps of the PCA analysis, calculation of difference spectra and the identification of WAMACs are not included in this research study, since it is already successfully performed and reported in previous publications [51,52,74].

Aquagrams were calculated at selected wavelengths of the 2nd overtone of OH, which showed the highest importance in the loadings of PCA, regression vectors of the PLSR models and difference spectra. These are the WAMACs for this particular work, wavelengths in the 2nd overtone of water at which water absorbance can be measured and provide the information of interest for water monitoring. However, the bands found to be influenced by humidity and temperature based on the results of PLSR analysis, were excluded from display, as they provide information about the change of water due to the changes in humidity and temperature, the factors that are not of interest and therefore risk a change in aquagram and signal that something occurred with water, when in fact this is not the case.

The selection of months for display of spectral patterns for groundwaters was based on the humidity and temperature variations in Wakayama, Japan where the Climate Data Wakayama was used as a data source from Climate-Data.org. R programing language (R Core Team, R: A Language and Environment for Statistical Computing, 2017) was used for calculation and visualization.

3. Results and discussion

3.1. Exploratory data evaluation

The distribution of the analyzed parameters has to be normal in case of the different tested water samples in order to perform a valid comparison. The temperature and environmental humidity values recorded at the times of measurement of groundwater samples along the three years were statistically evaluated prior to the spectral analysis.

The statistical analysis found no significant differences in the values of relative humidity of the environment nor for the temperature of the measured waters during any of the three years (Fig. 1). The results of the exploratory data evaluation also showed that there is a wide range of the measured parameters over the three-year monitoring period: the temperature values were between 15 and 30 °C while humidity ranged between 30 and 80%. This shows that there is enough variability in the datasets of examined parameters to ensure robust analysis of their effects on the molecular structure of examined groundwater samples and their blend.

3.2. Quantitative data analysis

The results of PLSR analysis using water temperature as a dependent variable, built separately using the spectral datasets acquired during Year 1 for each of the three analyzed waters, are shown in Fig. 2. Model parameters of PLSR showed the best agreement between measured and predicted values in the case of model developed for water W_{deep}. In model calibration (R^2_C = 0.9049, RMSEC = 1.09 °C) as well as in cross-validation (R^2_{CV} = 0.8927, RMSECV = 1.15 °C) very similar results were found for water W_{mix} and the weakest relationship between the water temperature and the NIR spectra of water was found for water $W_{shallow}$. Based on the pattern of errors that can be seen in Fig. 2 a) and d), for both

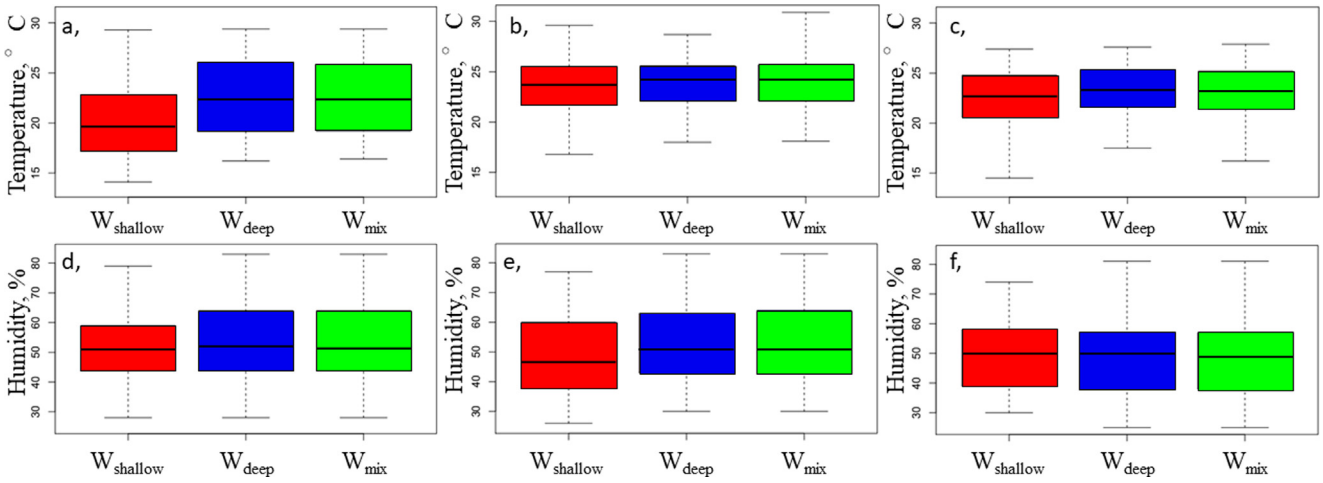

Fig. 1. Distribution of water temperature and relative humidity along the three years. a), b) and c) represent the distribution of water temperature and d), e) and f) represent the distribution of relative humidity during Year 1, Year 2 and Year 3, respectively. (Color figure).

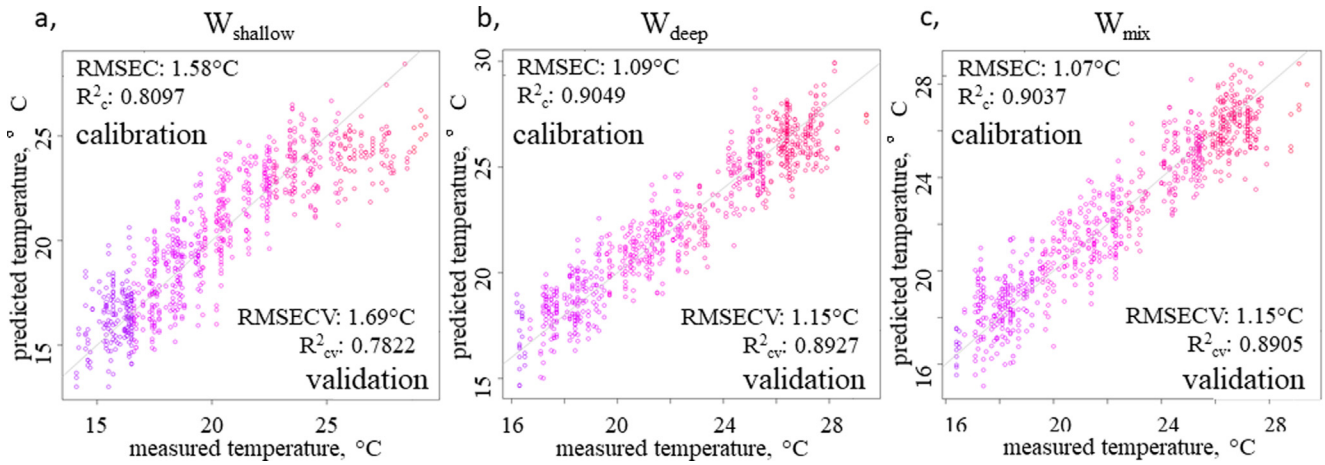

Fig. 2. Cross-validation results of PLSR models on water temperature based on data of Year 1. a), b) and c) validation Y-fit plots showing agreement between measured and predicted values of temperature using developed PLSR water temperature models for $W_{shallow}$, W_{deep} and W_{mix}, respectively (the number of spectra included in the analysis: $n_{shallow}$ = 849, n_{deep} = 868, n_{mix} = 850). Smoothed (2nd order polynomial filter and 11 points) and MSC transformed spectra of 600–1060 nm interval and 10 latent variables were used in all the three cases (leave-one-temperature level-out cross-validation). The color of data points reflects the change in values of recorded temperature from the lowest temperature (dark purple) to highest temperature (orange) **(Color figure)**.

calibration and validation respectively, the values of temperature predicted by the model tend to be lower than actual values, for the temperatures higher than 25 °C.

The regression vectors of the PLSR models built for water temperature are presented in Fig. 3. These regression vectors describe the relationship between the change of temperature and the spectral pattern of different waters. It is interesting to see the similarities in the main patterns of the regression vectors of different waters. It can be seen they are not the exactly the same and the differences between the regression vectors point out to the specificity of each water. The regression vectors for waters W_{deep} and W_{mix} were found to be more similar, which implies the stronger influence of W_{deep} on the spectral pattern of W_{mix} water. This may be understandable considering the rich mineral content of W_{deep}.

In PLSR, the observed response values are approximated by a linear combination of the values of the predictors. In our case, this means between the measured environmental parameters and absorbance at each wavelength of the measured spectra. The

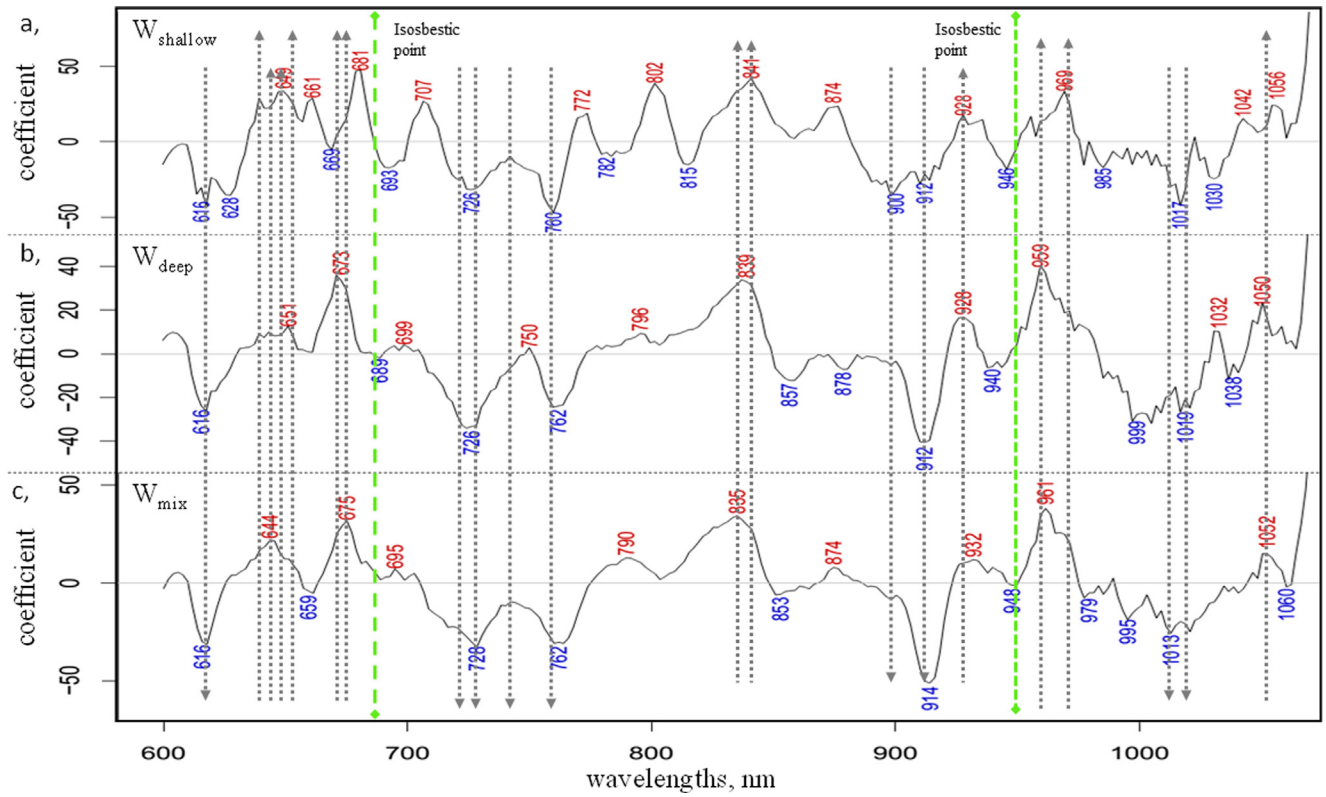

Fig. 3. Regression coefficient vectors of PLSR calibration models developed for water temperature as a dependent variable, using data of Year 1, a), b) and c) are regression coefficient vectors for W_{deep}, $W_{shallow}$ and W_{mix}, respectively (n_{deep} = 868, $n_{shallow}$ = 849, n_{mix} = 850). Smoothed (2nd order polynomials and 11 points) and MSC transformed spectra of 600–1060 nm interval and 10 latent variables were used in all the three cases (leave-one-temperature level-out cross-validation). **(Color figure)**.

coefficients in that combination, called regression coefficients, when represented on a regression vector plot can help identify the important wavelengths for the prediction of a measured response variable, which are in the case of this study, temperature and humidity, respectively.

The regression coefficient vectors, from the PLSR using temperature as a dependent variable, presented on Fig. 3 show several common upward (gray arrows pointing up) and downward peaks (gray arrows pointing down), suggesting that absorbance of each water changes in the same direction with the change in the temperature. The common downward peaks can be observed at 616 nm, 724–728 nm, 740 nm (trough), 760–762 nm, 900 nm, 912–914 nm, and 1013–1019 nm. Upward peaks can be found at 640 nm, 644 nm, 649 nm and 651 nm (seemingly one wide peak ~ 640–651 nm, but most probably composed of several overlapping peaks), 673–675 nm, 835–841 nm, 928–932 nm, 959–961 nm, and 1050 – 1056 nm. These absorbance bands can be considered sensitive to the changes in temperature, since they were found common for all three waters. Several existing literature sources have reported the bands close to 830–840 nm to be highly correlated with the sample temperature [75] (for example: 838 nm [76]; 841 nm [77]; 836 nm [65] and 837.5 nm [78]). Langford et al. 2001 by examining temperature dependence of pure liquid water in visible-near infrared spectrum also report peak maxima close to 836 nm, and the second one at 738 nm [65]. Cozzolino et al. 2007 reported that band at 966 nm changes linearly with the temperature, which may correspond to our 959–961 nm; the difference being due to different resolution of the instrument they used [79].

All three regression vectors passed the zero line at two points in the spectra: at 689 nm and 948 nm (indicated by green dashed lines at Fig. 3), suggesting that at these places the water absorbance is not influenced by the temperature of the ambient, i.e. that those may correspond to isosbestic points of 3rd and 2nd overtone

Table 2
Absorbance bands (nm) with regression coefficients of equal sign in PLSR models developed for prediction of temperature for three examined water types in the spectral region 600 – 1060 nm and their tentative assignments. The wavelengths given in the parentheses in the assignmens' column are the band positions from the cited literature and in the majority of cases recalculated from wavenumbers or overtones from fundamental frequencies reported in the original source. The overtones (λ) occurring at integer multiples (n) of fundamental vibrations (ν) are calculated from the mid infrared absorption bands using the following equation: $\lambda(nm) = \frac{10000000}{\nu(cm^{-1})}$.

Sign	Position (nm)	Tentative assignment
(-)	616	Unknown
(-)	724–728	(723 nm) maximum absorption peak of water vapor [82]
		(725.5 nm) 3rd overtone OH– stretch (OH–$(H_2O)_5$) [87]
		(726.2 nm) 4th overtone intermolecular hydrogen bond stretch (OH–$(H_2O)_3$) [99]
(-)	740	(739 nm) 3rd overtone of symmetric and asymmetric stretching vibration [83]
		(~740 nm) – peak in absorbance spectra of pure water with strong temperature dependency [84]
(-)	760–762	(757 nm) deionized water, 3rd overtone [85]
		(770 nm) maximum absorption peak of liquid water near freezing point [82]
(-)	900	(900.9 nm) 2nd overtone OH– stretch (OH–$(H_2O)_5$) [86]
		(900.9 nm) OH stretching 2nd overtone [87]
(-)	912–914	(912.46 nm)2nd overtone OH-stretch in OH-H_2O[86]
		(912.5 nm) free OH stretch in proton hydrate $H_{15}O_7$+, 2nd overtone [88]
		(913.0 nm) Proton hydrate $H_{17}O_8$+, 2nd overtone[88]
		(913.0 nm) free OH stretch in proton hydrate $H_{15}O_7$+, 2nd overtone [89]
		(913.0 nm) free OH stretch in proton hydrate $H_{17}O_8$+, 2nd overtone [89]
		(913.2 nm) H_2O symmetric stretch, in aqueous proton [H+·$(H_2O)_6$] – 2nd overt. [87]
		(913.73 nm) 2nd overtone (OH–$(H_2O)_5$) [86]
		(913.7 nm) $H_{13}O_6$ + free OH stretch, 2nd overt. [89]
		(914.0 nm) aqueous proton [H+·$(H_2O)_5$] - H_2O symmetric stretch, 2nd overt. [87]
		(914 nm) 2nd overtone Superoxide Tetrahydrate O_2–.$(H_2O)_4$ [90]
(-)	1013	(1010.1 nm)H_2O deionized, 2nd overt. [91]
		(1018.1 nm)hydrated proton [H+·$(H_2O)_6$] - H_2O symmetric stretch, 2nd overt. [87]
(-)	1019	(1018.1 nm)hydrated proton [H+·$(H_2O)_6$] - H_2O symmetric stretch, 2nd overt. [87]
(+)	640	(641 nm) Superoxide dihydrate $O_2^-(H_2O)_2$ – 4th overtone [90]
(+)	644	(645 nm) Superoxide trihydrate O_2– $(H_2O)_3$ 4th overtone[90]
(+)	649	Unknown
(+)	651	Unknown
(+)	673–675	(672.8 nm) proton hydrate $H_{17}O_8^+$, 3rd overt. [88 90]
		(673.1 nm) free OH stretch in proton hydrate $H_9O_4^+$, 3rd overt. [89]
		(673.1 nm) free OH stretch in proton hydrate $H_{17}O_8^+$, 3rd overt. [88]
		(673.3 nm) proton hydrate $H_{15}O_7^+$, 3rd overt. [87]
		(673.5 nm) proton hydrate $H_{11}O_5^+$ AD-type H_2O free OH stretch, 3rd overt. [89]
		(673.5 nm) free OH stretch in proton hydrate $H_{15}O_7$+, 3rd overt. [89]
		(673.9 nm) free OH stretch in proton hydrate $H_{13}O_6$+, 3rd overt. [89]
		(674.0 nm) free OH stretch in proton hydrate $H_{11}O_5$+, 3rd overt. [92]
		(675.7 nm) –OH free stretching, 3rd overt. [90]
		(675.68 nm) (OH–$(H_2O)_5$) 3rd overt.
(+)	835–841	(836 nm) 2nd overtone of the combination band of water av1 + v2 + bv3; a + b = 3 [83]
		(837 nm) $H_{13}O_6$ + H-bonded OH stretch, 3rd overt. [89]
		(837 nm) Water deionized [91]
		(841.5 nm) aqueous proton [H+·$(H_2O)_5$] - H_3O + symmetric stretch, 3rd overt. [87]
		(835 – 841 nm) Absorbance band of water highly influenced by temperature [65,76-79]
(+)	928–932	(926 nm) 3rd overtone IHB stretch (OH–$(H_2O)_2$) [86]
		(930.8 nm) H_9O_4 + H-bonded OH stretch, 3rd overt. [89]
		(931.1 nm) aqueous proton [H+·$(H_2O)_3$] - H_3O + free-OH stretch, 2nd overt. [87]
(+)	959–961	(960 nm) overtone of combination of the symmetric OH stretch and bending mode [93]
		(961.5 nm) 3rd overtone Superoxide Monohydrate O2–.$(H_2O)_1$ [90]
		(961.55 nm) 3rd overtone IHB stretch (OH–$(H_2O)_3$) [86]
(+)	1050–1056	(1054.9 nm) aqueous proton [H+·$(H_2O)_6$] - H_2O in H_5O_2 + symmetric stretch, 2nd overt. [87]
		(1054.9 nm) $H_{15}O_7$ + H-bonded OH stretch, 2nd overt. [89]

of water, respectively. The first one is close to the 772 nm as reported by Langford et al. 2001 who did not examine spectrum for wavelengths longer than 900 nm [65]. The slight position difference may be originating from differences in instruments, and also the purity of water (they worked with ultra-pure water). The greatest effect of temperature we observed at the bands that correspond to the peaks of the overtones and combination bands of water vibrations, around 740 nm, 840 nm and 960 nm which is in agreement with the literature [65,80,81].

The tentative assignments as well as the agreement with the existing literature sources for all the bands listed here are provided in the following table, Table2.

Relative humidity of the environment has significant impacts on near infrared absorption in general, being of particular importance for measurement accuracy of portable instruments in short wavelength range [94,95]. It can therefore be expected for humidity to exerts effects on the spectral pattern of water samples in the case of this study. The moisture in air has two different effects – it

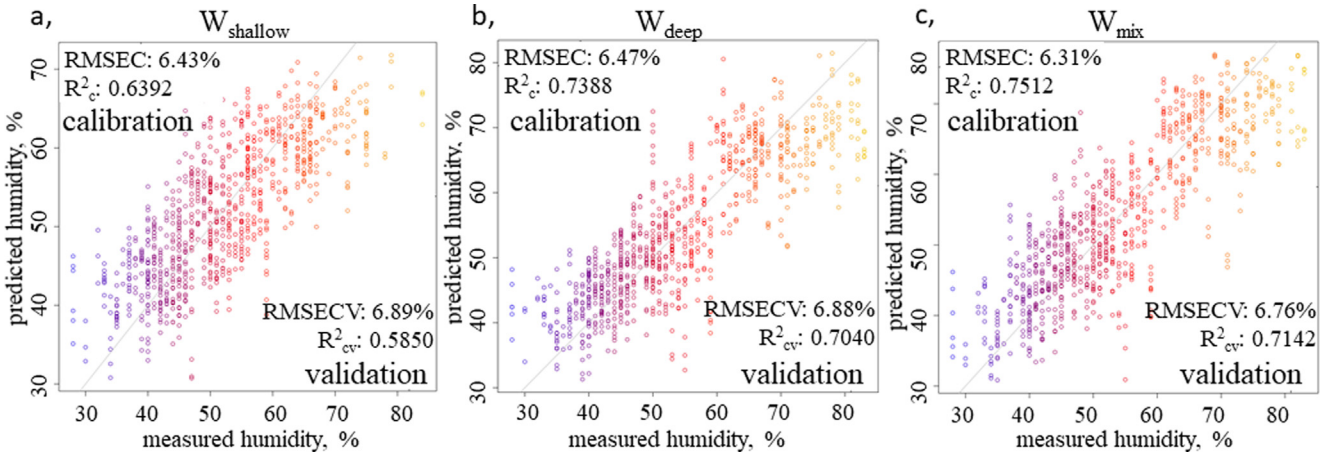

Fig. 4. Cross-validation results of PLSR models for relative humidity as a dependent variable, based on the data of Year 1. a), b) and c) validation Y-fit plots showing agreement between measured and predicted values of humidity using developed PLSR of relative humidity for $W_{shallow}$, W_{deep} and W_{mix}, respectively ($n_{shallow}$ = 849, n_{deep} = 868, n_{mix} = 850). Smoothed (2nd order polynomials and 11 points) and MSC transformed spectra of 600–1060 nm interval and 10 latent variables were used in all the three cases (leave-one-humidity level-out cross-validation). The color of data points reflects the change in values of recorded relative humidity from the lowest values (dark purple) to the highest (yellow) (Color figure).

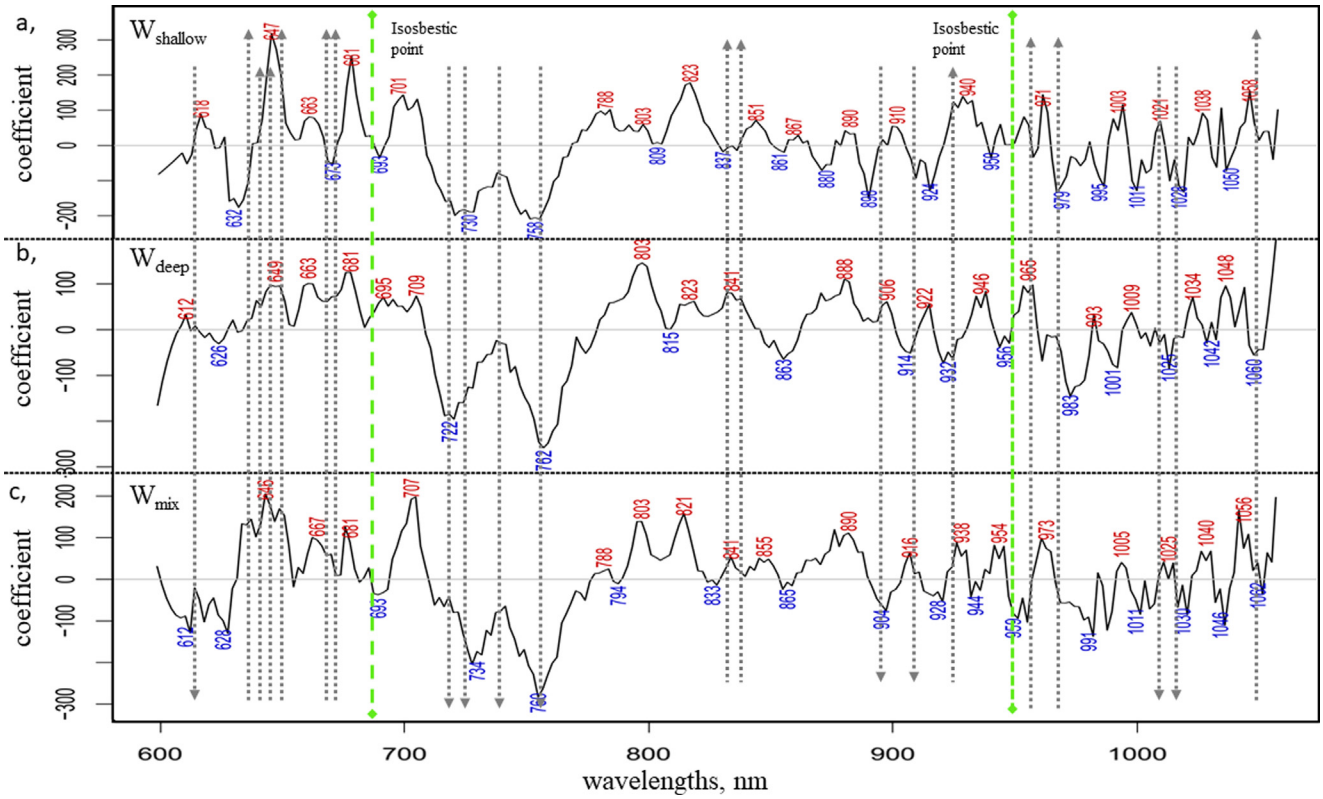

Fig. 5. Regression coefficient vectors of PLSR calibration models fitted on relative humidity based on data of Year 1, a), b) and c) are regression coefficient vectors for Wdeep, Wshallow and Wmix, respectively (ndeep = 868, nshallow = 849, nmix = 850). Smoothed (2nd order polynomials and 11 points) and MSC transformed spectra of 600–1060 nm interval and 10 latent variables were used in all the three cases (leave-one-humidity level-out cross-validation). (Color figure).

can affect the very samples and also through radiation scattering which leads to effects over the entire spectrum by shifting the baseline [96]. The results of PLSR analysis using humidity as a dependent variable and spectral data acquired during Year 1, separately for each of the three analyzed waters are shown in Fig. 4. Similar to the results of the temperature PLSR models, better results were obtained for waters W_{deep} and W_{mix} in model calibration as well as in cross-validation than for water $W_{shallow}$. Compared to the relationship of water absorbance and temperature, the linear relationship between absorbance and humidity is slightly weaker, suggesting lesser influence of humidity to spectral patterns compared to the temperature.

The regression coefficient vectors from the PLSR models of humidity as a dependent variable, are provided in Fig. 5.

The common upward peaks identified in regression vectors for all waters were found at: 646 – 649 nm, 663 – 667 nm, 681 nm, 701–709 nm, 788 nm, 803 nm, 821 – 823 nm, and 888 – 890 nm (indicated by gray arrows pointing up, Fig. 5). Common downward peaks were found at: 626 nm, 722 nm, 730–734 nm, 740 nm, 758–762 nm, 861 – 865 nm, 979 nm, 1015 nm, 1028 – 1030 nm, 1042 nm (indicated by gray arrows pointing down, Fig. 5). The common sign in regression coefficient in models for humidity developed based on spectral data for each water suggests the same direction of changes in absorbance at those bands with changes in relative humidity. The tentative assignments based on the existing literature sources of these bands is provided in Table3.

The regression vectors of PLSR models developed for the temperature and humidity based on the spectral data collected during the next two years resulted in the similar absorbance bands (data not shown) therefore the next part of the analysis was focused on qualitative evaluation of groundwaters.

3.3. Qualitative data evaluation

The water spectral patterns of the different groundwater samples depicted at WAMACS wavelengths are demonstrated with their aquagrams showing the data of the three years separately in Fig. 6. The WAMACs axes were selected from the wavelengths found important in PCA (data not shown), PLSR and subtracted spectra, for the description of the analyzed waters, but excluding those found most affected by temperature and humidity in the environment, resulting in the following wavelengths: 902 nm, 912 nm, 924 nm, 940 nm, 958 nm, 975 nm, 991 nm, 1005 nm, 1015 nm, 1038 nm, 1046 nm, 1050 nm that correspond to water absorbance bands with the assignments as provided in Table 4.

We have here selected for display the aquagrams for the 3 waters generated as averaged for each of the following four months: June, July, August and September. These four months correspond to the summer time in Japan, during which the temperature and humidity of the environment are at their highest variations. June being the month with the highest number of rainy days in a year, followed by July when the humidity is at its peak, and August when the temperature reaches the highest values in Wakayama (Climate Data Wakayama from Climate-Data.org. [102]). As one research study found, the joint impact of high temperature/ high relative humidity had led to highest impacts and deviations in the measurements of portable, short wavelength infrared devices [94].

However, despite influences from environmental temperature and humidity, or other environmental factors on water, aquagrams calculated based on the independent data of the three different years show very consistent spectral patterns of the tested waters (Fig. 6).

Based on the provided assignments in Table 4, it can be seen that the part of aquagrams from 902 nm to 975 nm correspond to free OH stretch in solvation shells and hydrated proton clusters, while the rest of the bands correspond to absorption of hydrogen bonded OH in solvation shells and hydrated proton clusters. This means, that, in general, we can observe higher absorbance values for W_{deep} and W_{mix} waters at both lower wavelengths referring to less hydrogen bonded structures and high wavelengths corresponding to more hydrogen bonded water. On the contrary $W_{shallow}$ water presents lower absorbance free water molecules around 940 nm and higher absorbance values mainly around 992 nm showing higher concentration of water molecular species with four hydrogen bonds. Possible reasons to explain this phenomenon could be the different electroconductivity and mineral content of the groundwaters, Table 1. Water $W_{shallow}$ coming from shallower source has lower electroconductivity and mineral content than water W_{deep} originated from deeper source and W_{mix} which is their mixture. The finding that increasing concentration of minerals causes increase in less H-bonded water molecular network is in good agreement with the results of previous researches [22,105-107]. These results confirm that the approach employed

Table 3
Absorbance bands (nm) with regression coefficients of equal sign in PLSR models developed for prediction of relative humidity of the environment during spectral measurements of three examined waters in the spectral region 600 – 1060 nm and their tentative assignments. The wavelengths given in the parentheses in the assignment column are the band positions from the cited literature and in the majority of cases recalculated from wavenumbers or calculated overtones from fundamental frequencies reported in the original source. The overtones (λ) occurring at integer multiples (n) of fundamental vibrations (ν) are calculated from the mid infrared absorption bands using the following equation: $\lambda(\boldsymbol{nm}) = \frac{10000000}{\nu(\boldsymbol{cm^{-1}})}$.

Sign	Position (nm)	Tentative assignment
(-)	626	Unknown
(-)	722	(721.5 nm) H_2O, 3rd overt. [91] (723 nm) maximum absorption peak of water vapor [82]
(-)	730–734	(732.6 nm) 4th overtone Superoxide Tetrahydrate O_2–.(H_2O) [90] (735.3 nm) Hydrogen-bonded –OH, 3rd overt. [97]
(-)	740	Maximum absorption peak of liquid water near boiling point [82]
(-)	758–762	(757.5 nm) 3rd overtone Superoxide Tetrahydrate O_2–.(H_2O)$_4$[90] (757.6 nm) H_2O deionized, 3rd overt. [91]
(-)	861–865	(860 nm) 3rd overtone IHB stretch (OH–(H_2O)$_3$) [98] (862 nm) 3rd overtone IHB stretch (OH–(H_2O)$_4$) [86] (862.1 nm) H_3O^+, 3rd overt. [99]
(-)	979	(980 nm) hydroxide ion [93] (980.4 nm) Hydrogen-bonded –OH, 2nd overt. [97]
(-)	1015	(1010 nm) 2nd overtone Superoxide Tetrahydrate O_2–.(H_2O)$_4$ [90] (1010.1 nm) H_2O deionized, 2nd overt. [91] (1018.1 nm) aqueous proton [H^+·(H_2O)$_6$] - H_2O in $H_5O_2^+$ symmetric stretch, 2nd overt. [87]
(-)	1028–1030	Unknown
(-)	1042	(1041.3 nm)$H_{11}O_5^+$ H-bonded OH stretch, 2nd overt. [89] (1041.7 nm)Hydrogen-bonded –OH, 2nd overt. [97] (1043.3 nm)aqueous proton [H+·(H_2O)$_5$] – Acceptor-Donor-type H_2O H-bond stretch, 2nd overt. [87]
(+)	646–649	(645 nm) 4th overtone IHBstr/HOH bend (OH-H_2O) [86] (645.2 nm) 4th overtone Superoxide Tetrahydrate O_2–.(H_2O)$_3$ [90]
(+)	663–667	(665.6 nm) H_2O v_3, 3rd overt. [100]
(+)	681	3rd overtone free OH stretch (OH–(H_2O)$_4$) [86] 3rd overtone free water OH stretch (OH-H_2O) [98]
(+)	701–709	(703.6 nm) $H_{15}O_7$ + H-bonded OH stretch, 3rd overt. [89] (706.8 nm) 4th overtone Superoxide Tetrahydrate O_2–.(H_2O)$_3$ [90]
(+)	788	(791.1 nm)aqueous proton [H^+·(H_2O)$_6$] - H_2O in $H_5O_2^+$ symmetric stretch, 3rd overt. [87] (791.1 nm)$H_{15}O_7^+$ H-bonded OH stretch, 3rd overt. [89]
(+)	803	(800 nm) maximum absorption peak for ice [82]
(+)	821–823	Unknown
(+)	888–890	(887.5 nm)H_2O v_3, 2nd overt. [100]

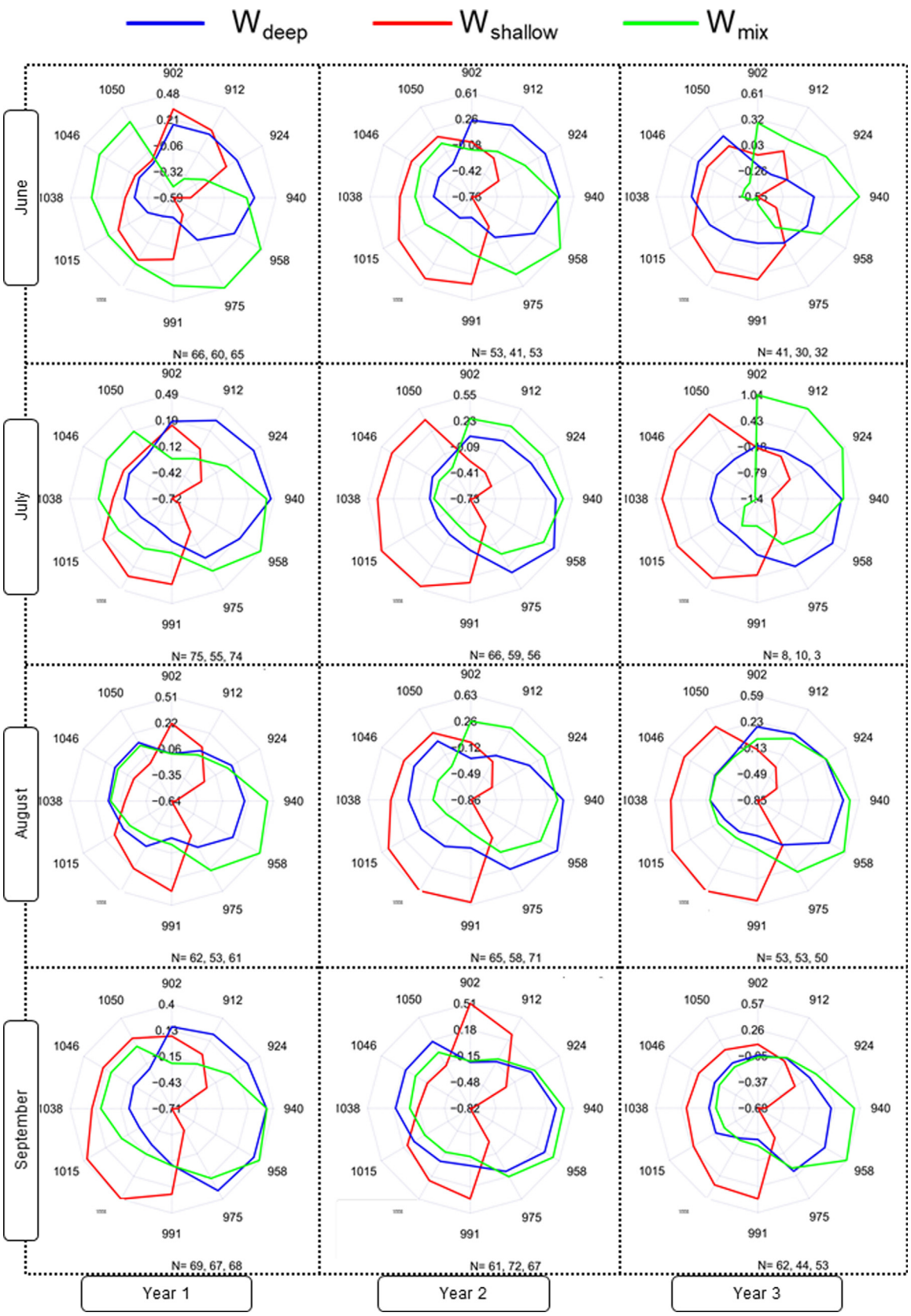

Fig. 6. Aquagrams of groundwater samples W_{deep}, $W_{shallow}$ and their blend W_{mix}, presenting their spectral patterns in the water second overtone during four months June, July, August and September, when the temperature and humidity in the environment are at their highest, for all three consecutive years of monitoring (N – number of spectra used for calculation of the aquagram for the waters in the following order - N_{deep}, $N_{shallow}$, N_{mix} (Color figure).

Table 4
The position and tentative assignments of WAMACs that can be used for the description of the state of analyzed waters, excluding those found most affected by temperature and humidity in the environment. The wavelengths given in the parentheses in the assignment column are the closest band positions from the cited literature and in the majority of cases recalculated from wavenumbers or calculated overtones from fundamental frequencies reported in the original source. The overtones (λ) occurring at integer multiples (n) of fundamental vibrations (ν) are calculated from the mid infrared absorption bands using the following equation: $\lambda(nm) = \frac{10000000}{\nu(cm^{-1})}$.

Position (nm)	Assignment
902	(902.1 nm) — non-bonded OH stretch, 2nd overtone [87] (902.13 nm) — free OH stretch in solvation shell OH–$(H_2O)_3$, 2nd overt. [86] (902.36 nm) – free OH stretch in solvation shell OH–$(H_2O)_2$, 2nd overt. [86]
912	(912.46 nm) — free OH stretch in solvation shell OH–(H_2O), 2nd overt. [86] (912.5 nm) – hydrated proton clusters $H^+ \cdot (H_2O)_7$, 2nd over. [88]
924	(922.1 nm) — solvation shell (OH–$(H_2O)_4$), 2nd overt. [87] (925.9 nm) — hydrated proton cluster $H^+ \cdot (H_2O)_{10}$, 2nd overt.[92]
940	(938.2 nm) - hydrated proton cluster $H^+ \cdot (H_2O)_7$, 2nd overt.[89] (942 nm) — water vapour [82]
958	(958 nm) — moisture [14]
975	(976 nm) — bulk water [101]
991	(990 nm) — intramolecular hydrogen bonded OH stretch in (OH–$(H_2O)_3$) or (OH–$(H_2O)_4$), 2nd overt. [98] (991.2 nm) — hydrogen-bonded OH stretch in hydrated proton cluster $H^+ \cdot (H_2O)_7$, 2nd overt.[89]
1005	(1004.0 nm) – H-bonded OH stretch in hydrated proton cluster $H^+ \cdot (H_2O)_6$, 2nd overt.[87] (1005.8 nm) – H-bonded OH stretch in hydrated proton cluster $H^+ \cdot (H_2O)_6$, 2nd overt [89]
1038	(1041.3 nm) - H-bonded OH stretch in $H^+ \cdot (H_2O)_5$, 2nd overt.[89] (1041.7 nm) — H-bonded OH stretch in hydrogen-bonded –OH, 2nd overt.[97]
1046	(1043.3 nm) — H-bonded OH stretch in hydrated proton cluster $H^+ \cdot (H_2O)_5$, 2nd overt.[87]
1050	(1054.9 nm) — hydrated proton cluster H+·(H2O)6, 2nd overt. [87] (1054.9 nm) — H-bonded OH stretch in hydrated proton cluster $H^+ \cdot (H_2O)_7$, 2nd overt.[89]

by the Aquaphotomics evaluation technique, namely using water as a mirror instead of specific measurements of the individual components dissolved in water, can provide an indicator of possible changes in the water composition based on the spectra in the short wavelength near infrared range [52].

Taken together, these results show that each water sample, can be characterized successfully by its spectral pattern, distinctive for each ground water and their mix. The differences in spectral pattern, after elimination of the absorbance bands highly influenced by temperature and humidity changes of the environment, present stable, easily identifiable pattern for each water. It can serve as a comprehensive marker of the state of the water as an integral system (water + solutes), that is stable against seasonal changes in the environment and will change only in response to changes in water mineral content and/or undesirable circumstances during extraction process which may result in the loss of desired quality. Instead of performing numerous, off-line, discrete measurements of individual physico-chemical parameters, the proposed aquaphotomics approach provides real-time monitoring solution for cost effective screening of water that can indicate when something occurs that would require more in-depth analysis. Considering the trend of miniaturization and decreased costs of near infrared spectroscopic systems, and the fact that results obtained here utilized short wavelength region, it can be concluded that the proposed solution may result in development of low-cost portable, miniature sensors that can be easily integrated into any water production or water treatment system to enable real-time quality screening.

4. Conclusions

The results of groundwater samples with different mineral content and electroconductivity showed that surrounding temperature and humidity have a great influence on their visible and near-infrared spectra. The influence of these two environmental factors show some common spectral features for the different waters, suggesting the impact on the measurement process, but also some differences showing that each water sample is perturbed in a specific way. The common bands that were particularly affected by temperature and humidity were identified in each of the spectral patterns. Selection of water matrix coordinates, absorbance bands at which the absorbance of the samples should be measured in order to provide stable spectral pattern was performed. The spectral patterns of each analyzed water show consistent, stable features in 3 years of monitoring, during months when the temperature and relative humidity of the environment are at their highest variation. The water spectral patterns can still easily distinguish between each of the water sample, signature-like markers that can be used for monitoring. This specific quality of different waters can be explained by their specific mineral content. These results confirm that short wavelength near infrared spectral pattern of water can be used for water screening practice to indicate occurrence of changes in the water that would require more in-depth analysis.

Real-time, online system based on the aquaphotomics near infrared spectroscopy could present an efficient, practical approach for monitoring of quality of water during treatment as well as at the point of use, signaling the changes in water quality based on detection of changes in water structure.

CRediT authorship contribution statement

Zoltan Kovacs: Conceptualization, Methodology, Software, Validation, Formal analysis, Data curation, Investigation, Writing – original draft, Writing – review & editing, Visualization. **Jelena Muncan:** Formal analysis, Validation, Writing – review & editing, Visualization. **Petya Veleva:** Formal analysis, Writing – original draft, Visualization. **Mitsue Oshima:** Resources, Investigation. **Shogo Shigeoka:** Conceptualization, Resources, Project administration, Funding acquisition. **Roumiana Tsenkova:** Conceptualization, Methodology, Validation, Resources, Writing – review & editing, Data curation, Supervision, Project administration, Funding acquisition.

Declaration of Competing Interest

The authors declare that they have no known competing financial interests or personal relationships that could have appeared to influence the work reported in this paper.

Acknowledgements

Authors J.M. and P.V. gratefully acknowledge the support of Japanese Society for Promotion of Science (P17406 and PE15026). Author Z. K. gratefully acknowledges the support by the European Social Fund (grant agreement no. EFOP-3.6.3-VEKOP-16-2017-00005).

References

[1] A.G. Császár, G. Czakó, T. Furtenbacher, J. Tennyson, V. Szalay, S.V. Shirin, N.F. Zobov, O.L. Polyansky, On equilibrium structures of the water molecule, J. Chem. Phys. 122 (21) (2005) 214305.
[2] A.H. Harvey, D.G. Friend, Physical Properties of Water, in: D. Palmer, R. Fernandez-Prini, A. Harvey (Eds.), Aqueous Syst. Elev. Temp. Press. Phys.

Chem. Water, Steam Hydrothermal Solut., Elsevier Ltd, London, UK, 2004: pp. 1–29.
[3] C.M. Porth, Essentials of pathophysiology: Concepts of altered health states, 3rd ed., Wolters Kluwer Health | Lippincott Wlliams & Wilkins, 2011.
[4] E. Viala, Water for food, water for life a comprehensive assessment of water management in agriculture, Irrig. Drain. Syst. 22 (2008) 127–129, https://doi.org/10.1007/s10795-008-9044-8.
[5] M.H. Banna, S. Imran, A. Francisque, H. Najjaran, R. Sadiq, M. Rodriguez, M. Hoorfar, Online Drinking Water Quality Monitoring: Review on Available and Emerging Technologies, Crit. Rev. Environ. Sci. Technol. 44 (12) (2014) 1370–1421.
[6] H. Zhao, D. Jiang, S. Zhang, K. Catterall, R. John, Development of a Direct Photoelectrochemical Method for Determination of Chemical Oxygen Demand, Anal. Chem. 76 (1) (2004) 155–160.
[7] C. Chow, S.D. Thomas, D.E. Davey, D.E. Mulcahy, M. Drikas, Development of an on-line electrochemical analyser for trace level aluminium, Anal. Chim. Acta. 499 (2003) 173–181, https://doi.org/10.1016/j.aca.2003.08.028.
[8] S. Winkler, L. Rieger, E. Saracevic, A. Pressl, G. Gruber, Application of ion-sensitive sensors in water quality monitoring, Water Sci. Technol. 50 (2004) 105–114.
[9] R. O'Halloran, S. Fogelman, H. Zhao, Current Online Water Quality Monitoring Methods and Their Suitability for the Western Corridor Purified Recycled Water Scheme. Urban Water Security Research Alliance Technical Report No. 10., Queensland, 2009.
[10] O. Korostynska, A. Mason, M. Ortoneda-Pedrola, A. Al-Shamma'a, Electromagnetic wave sensing of NO3 and COD concentrations for real-time environmental and industrial monitoring, Sensors Actuators B Chem. 198 (2014) 49–54. https://doi.org/10.1016/j.snb.2014.03.030.
[11] P. Ball, Water is an activematrix of life for cell and molecular biology, Proc. Natl. Acad. Sci. U. S. A. 114 (2017) 13327–13335, https://doi.org/10.1073/pnas.1703781114.
[12] J. Muncan, R. Tsenkova, Aquaphotomics-From Innovative Knowledge to Integrative Platform in Science and Technology, Molecules 24 (2019) 2742, https://doi.org/10.3390/molecules24152742.
[13] R. Tsenkova, Aquaphotomics: Dynamic spectroscopy of aqueous and biological systems describes peculiarities of water, J. Near Infrared Spectrosc. 17 (2009) 303–313, https://doi.org/10.1255/jnirs.869.
[14] P. Williams, K. Norris, Near-Infrared Technology in the Agricultural and Food Industry, 2nd ed., American Association of Cereal Chemists Inc, Minnesota, USA, 2001.
[15] M. Blanco, I. Villarroya, NIR spectroscopy: a rapid-response analytical tool, TrAC, Trends Anal. Chem. 21 (2002) 240–250, https://doi.org/10.1016/S0165-9936(02)00404-1.
[16] E.B. van de Kraats, J. Munćan, R.N. Tsenkova, Aquaphotomics – Origin, concept, applications and future perspectives, Substantia. (2019) 13–28. https://doi.org/10.13128/substantia-702.
[17] A.A.A. Gowen, F. Marini, Y. Tsuchisaka, S. De Luca, M. Bevilacqua, C. O'Donnell, G. Downey, R. Tsenkova, C. O'Donnell, G. Downey, R. Tsenkova, On the feasibility of near infrared spectroscopy to detect contaminants in water using single salt solutions as model systems, Talanta 131 (2015) 609–618, https://doi.org/10.1016/J.TALANTA.2014.08.049.
[18] G. Bázár, Z. Kovacs, M. Tanaka, A. Furukawa, A. Nagai, M. Osawa, Y. Itakura, H. Sugiyama, R. Tsenkova, Water revealed as molecular mirror when measuring low concentrations of sugar with near infrared light, Anal. Chim. Acta. 896 (2015) 52–62, https://doi.org/10.1016/J.ACA.2015.09.014.
[19] H. Meilina, H. Meilina, A. Putra, R. Tsenkova, Frequency of use minute concentrations of cadmium in aqueous solution by near infrared spectroscopy and aquaphotomics, Proc. Annu. Int. Conf. Syiah Kuala Univ. - Life Sci. Eng. Chapter. 1 (2011). http://www.jurnal.unsyiah.ac.id/AICS-SciEng/article/view/1972 (accessed December 17, 2020).
[20] R. Tsenkova, Aquaphotomics: The extended water mirror effect explains why small concentrations of protein in solution can be measured with near infrared light, NIR News. 19 (2008) 13–14, https://doi.org/10.1255/nirn.1079.
[21] A. Putra, F. Faridah, E. Inokuma, R. Santo, Robust spectral model for low metal concentration measurement in aqueous solution reveals the importance of water absorbance bands, J. Sains Dan Teknol. Reaksi. 8 (2010). http://e-jurnal.pnl.ac.id/index.php/JSTR/article/view/105 (accessed August 9, 2018).
[22] A.A. Gowen, J.M. Amigo, R. Tsenkova, Characterisation of hydrogen bond perturbations in aqueous systems using aquaphotomics and multivariate curve resolution-alternating least squares, Anal. Chim. Acta. 759 (2013) 8–20, https://doi.org/10.1016/j.aca.2012.10.007.
[23] D. Kojić, R. Tsenkova, K. Tomobe, K. Yasuoka, M. Yasui, Water confined in the local field of ions, ChemPhysChem 15 (2014) 4077–4086, https://doi.org/10.1002/cphc.201402381.
[24] S. Tanaka, D. Kojić, R. Tsenkova, M. Yasui, Quantification of anomeric structural changes of glucose solutions using near-infrared spectra, Carbohydr. Res. 463 (2018) 40–46, https://doi.org/10.1016/J.CARRES.2018.04.012.
[25] L. Wang, X. Zhu, W. Cai, X. Shao, Understanding the role of water in the aggregation of poly(: N, N -dimethylaminoethyl methacrylate) in aqueous solution using temperature-dependent near-infrared spectroscopy, Phys. Chem. Chem. Phys. 21 (2019) 5780–5789, https://doi.org/10.1039/c8cp07153e.
[26] L. Ma, X. Cui, W. Cai, X. Shao, Understanding the function of water during the gelation of globular proteins by temperature-dependent near infrared spectroscopy, Phys. Chem. Chem. Phys. 20 (2018) 20132–20140, https://doi.org/10.1039/c8cp01431k.
[27] R.N. Tsenkova, I.K. Iordanova, K. Toyoda, D.R. Brown, Prion protein fate governed by metal binding, Biochem. Biophys. Res. Commun. 325 (2004) 1005–1012, https://doi.org/10.1016/j.bbrc.2004.10.135.
[28] Q. Dong, X. Guo, L. Li, C. Yu, L. Nie, W. Tian, H. Zhang, S. Huang, H. Zang, Understanding hyaluronic acid induced variation of water structure by near-infrared spectroscopy, Sci. Rep. 10 (2020) 1–8, https://doi.org/10.1038/s41598-020-58417-5.
[29] N. Goto, G. Bazar, Z. Kovacs, M. Kunisada, H. Morita, S. Kizaki, H. Sugiyama, R. Tsenkova, C. Nishigori, Detection of UV-induced cyclobutane pyrimidine dimers by near-infrared spectroscopy and aquaphotomics, Sci. Rep. 5 (2015) 11808, https://doi.org/10.1038/srep11808.
[30] G. Bázár, R. Romvári, A. Szabó, T. Somogyi, V. Éles, R. Tsenkova, NIR detection of honey adulteration reveals differences in water spectral pattern, Food Chem. 194 (2016) 873–880, https://doi.org/10.1016/j.foodchem.2015.08.092.
[31] M. Brambilla, M. Buccheri, M. Grassi, A. Stellari, M. Pazzaglia, E. Romano, T.M. P. Cattaneo, The influence of the presence of borax and NaCl on water absorption pattern during sturgeon caviar (Acipenser transmontanus) storage, Sensors (Switzerland). 20 (2020) 1–7, https://doi.org/10.3390/s20247174.
[32] S. Atanassova, Near Infrared Spectroscopy and aquaphotomics for monitoring changes during yellow cheese ripening, Agric, Sci. Technol. 7 (2015) 269–272.
[33] J. Muncan, K. Tei, R. Tsenkova, Real-time monitoring of yogurt fermentation process by aquaphotomics near-infrared spectroscopy, Sensors (Switzerland). 21 (2021) 1–18, https://doi.org/10.3390/s21010177.
[34] J. Muncan, Z. Kovacs, B. Pollner, K. Ikuta, Y. Ohtani, F. Terada, R. Tsenkova, Near infrared aquaphotomics study on common dietary fatty acids in cow's liquid, thawed milk, Food Control 122 (2020), https://doi.org/10.1016/j.foodcont.2020.107805 107805.
[35] X. Yang, P. Guang, G. Xu, S. Zhu, Z. Chen, F. Huang, Manuka honey adulteration detection based on near-infrared spectroscopy combined with aquaphotomics, Lwt. 132 (2020), https://doi.org/10.1016/j.lwt.2020.109837 109837.
[36] H. Kaur, R. Künnemeyer, A. McGlone, Investigating aquaphotomics for temperature-independent prediction of soluble solids content of pure apple juice, J. Near Infrared Spectrosc. 28 (2) (2020) 103–112.
[37] J. Muncan, B. Aouadi, F. Vitalis, Z. Kovacs, R. Tsenkova, Soil Aquaphotomics for Understanding Soil-Health Relation through Water-Light Interaction, Soil-Human Heal. Nexus. (2020) 197–221, https://doi.org/10.1201/9780367822736-10.
[38] H. Morita, T. Hasunuma, M. Vassileva, R. Tsenkova, A. Kondo, Near infrared spectroscopy as high-throughput technology for screening of xylose-fermenting recombinant Saccharomyces cerevisiae strains, Anal. Chem. 83 (2011) 4023–4029, https://doi.org/10.1021/ac103128p.
[39] H. Morita, T. Hasunuma, M. Vassileva, A. Kondo, R. Tsenkova, A new screening method for recombinant Saccharomyces cerevisiae strains based on their xylose fermentation ability measured by near infrared spectroscopy, Anal. Methods. 6 (2014) 6628–6634, https://doi.org/10.1039/c4ay00785a.
[40] A. Slavchev, Z. Kovacs, H. Koshiba, G. Bazar, B. Pollner, A. Krastanov, R. Tsenkova, Monitoring of water spectral patterns of lactobacilli development as a tool for rapid selection of probiotic candidates, J. Near Infrared Spectrosc. 25 (2017) 423–431, https://doi.org/10.1177/0967033517741133.
[41] A. Slavchev, Z. Kovacs, H. Koshiba, A. Nagai, G. Bázár, A. Krastanov, Y. Kubota, R. Tsenkova, G.-J. Nychas, Monitoring of water spectral pattern reveals differences in probiotics growth when used for rapid bacteria selection, PLoS ONE 10 (7) (2015) e0130698.
[42] B. Jinendra, K. Tamaki, S. Kuroki, M. Vassileva, S. Yoshida, R. Tsenkova, Near infrared spectroscopy and aquaphotomics: Novel approach for rapid in vivo diagnosis of virus infected soybean, Biochem. Biophys. Res. Commun. 397 (2010) 685–690, https://doi.org/10.1016/j.bbrc.2010.06.007.
[43] S. Kuroki, R. Tsenkova, D.P. Moyankova, J. Muncan, H. Morita, S. Atanassova, D. Djilianov, Water molecular structure underpins extreme desiccation tolerance of the resurrection plant Haberlea rhodopensis, Sci. Rep. 9 (2019) 3049, https://doi.org/10.1038/s41598-019-39443-4.
[44] K. Kinoshita, N. Kuze, T. Kobayashi, E. Miyakawa, H. Narita, M. Inoue-Murayama, G. Idani, R. Tsenkova, Detection of urinary estrogen conjugates and creatinine using near infrared spectroscopy in Bornean orangutans (Pongo Pygmaeus), Primates 57 (2016) 51–59, https://doi.org/10.1007/s10329-015-0501-3.
[45] K. Kinoshita, M. Miyazaki, H. Morita, M. Vassileva, C. Tang, D. Li, O. Ishikawa, H. Kusunoki, R. Tsenkova, Spectral pattern of urinary water as a biomarker of estrus in the giant panda, Sci. Rep. 2 (2012) 856, https://doi.org/10.1038/srep00856.
[46] G. Takemura, G. Bázár, K. Ikuta, E. Yamaguchi, S. Ishikawa, A. Furukawa, Y. Kubota, Z. Kovács, R. Tsenkova, Aquagrams of raw milk for oestrus detection in dairy cows, Reprod. Domest. Anim. 50 (2015) 522–525, https://doi.org/10.1111/rda.12504.
[47] R. Tsenkova, S. Atanassova, S. Kawano, K. Toyoda, Somatic cell count determination in cow's milk by near-infrared spectroscopy: a new diagnostic tool., J. Anim. Sci. 79 (2001) 2550–2557. http://www.ncbi.nlm.nih.gov/pubmed/11721833 (accessed February 19, 2019).
[48] J. Šakota Rosić, J. Munćan, I. Mileusnić, B. Kosić, L. Matija, Detection of protein deposits using NIR spectroscopy, Soft Mater. 14 (2016) 264–271, https://doi.org/10.1080/1539445X.2016.1198377.
[49] J. Munćan, J. Rosić, I. Mileusnić, V. Matović, L. Matija, R. Tsenkova, The structure of water in soft contact lenses: near infrared spectroscopy and

Aquaphotomics study, in: 18th Int. Conf. Near Infrared Spectrosc., IM Publications Open LLP, 2019: pp. 99–104. https://doi.org/10.1255/nir2017.099.
[50] L.R. Matija, R.N. Tsenkova, M. Miyazaki, K. Banba, J.S. Muncan, Aquagrams: Water spectral pattern as characterization of hydrogenated nanomaterial, FME Trans. 40 (2012) 51–56.
[51] J. Muncan, V. Matovic, S. Nikolic, J. Askovic, R. Tsenkova, Aquaphotomics approach for monitoring different steps of purification process in water treatment systems, Talanta 206 (2020), https://doi.org/10.1016/j.talanta.2019.120253 120253.
[52] Z. Kovacs, G. Bázár, M. Oshima, S. Shigeoka, M. Tanaka, A. Furukawa, A. Nagai, M. Osawa, Y. Itakura, R. Tsenkova, Water spectral pattern as holistic marker for water quality monitoring, Talanta 147 (2015) 598–608, https://doi.org/10.1016/j.talanta.2015.10.024.
[53] J. Muncan, L. Matija, J. Simic-Krstic, S. Nijemcevic, D. Koruga, Discrimination of mineral waters using near-infrared spectroscopy and aquaphotomics, Hem. Ind. 68 (2) (2014) 257–264.
[54] A.A. Gowen, Y. Tsuchisaka, C. O'Donnell, R. Tsenkova, Investigation of the potential of near infrared spectroscopy for the detection and quantification of pesticides in aqueous solution, Am. J. Anal. Chem. 2 (2011) 53–62, https://doi.org/10.4236/ajac.2011.228124.
[55] V. Bozhynov, P. Soucek, A. Barta, P. Urbanova, D. Bekkozhayeva, Visible aquaphotomics spectrophotometry for aquaculture systems, in: Springer, Cham, 2018: pp. 107–117. https://doi.org/10.1007/978-3-319-78723-7_9.
[56] R.C. Dougherty, L.N. Howard, Equilibrium structural model of liquid water: Evidence from heat capacity, spectra, density, and other properties, J. Chem. Phys. 109 (17) (1998) 7379–7393.
[57] B. Czarnik-Matusewicz, S. Pilorz, Study of the temperature-dependent near-infrared spectra of water by two-dimensional correlation spectroscopy and principal components analysis, Vib. Spectrosc. 40 (2006) 235–245, https://doi.org/10.1016/j.vibspec.2005.10.002.
[58] Y. Jin, S.-I. Ikawa, Near-infrared spectroscopic study of water at high temperatures and pressures, J. Chem. Phys. 119 (23) (2003) 12432–12438.
[59] M. Falk, T.A. Ford, Infrared spectrum and structure of liquid water, Https://Doi.Org/10.1139/V66-255. 44 (2011) 1699–1707, https://doi.org/10.1139/V66-255.
[60] S. Šašić, V.H. Segtnan, Y. Ozaki, Self-modeling curve resolution study of temperature-dependent near-infrared spectra of water and the investigation of water structure, J. Phys. Chem. A. 106 (2002) 760–766, https://doi.org/10.1021/jp013436p.
[61] V.H. Segtnan, T. Isaksson, Y. Ozaki, Studies on the Structure of Water Using Spectroscopy and Principal Component Analysis, Anal. Chem. 73 (2001) 3153–3161, https://doi.org/10.1021/ac010102n.
[62] Z. Kovacs, B. Pollner, G. Bazar, J. Muncan, R. Tsenkova, A Novel Tool for Visualization of Water Molecular Structure and Its Changes, Expressed on the Scale of Temperature Influence, Molecules. 25 (2020) 2234, https://doi.org/10.3390/molecules25092234.
[63] J. Muncan, D. Koruga, Study of the structure of water under influence of temperature and pressure, in: V. Bellon-Maurel, P. Williams, G. Downey (Eds.), NIR2013 Proc, Pick. Up Good Vib, ICNIRS, La Grande-Motte, France, 2013, pp. 588–594.
[64] A. Nilsson, L.G.M. Pettersson, The structural origin of anomalous properties of liquid water, Nat. Commun. 6 (1) (2015), https://doi.org/10.1038/ncomms9998.
[65] V.S. Langford, A.J. McKinley, T.I. Quickenden, Temperature dependence of the visible-near-infrared absorption spectrum of liquid water, J. Phys. Chem. A. 105 (2001) 8916–8921, https://doi.org/10.1021/jp010093m.
[66] V.H.V. Segtnan, Š. Šašić, T. Isaksson, Y. Ozaki, S. Šašić, T. Isaksson, Y. Ozaki, S. Sasic, T. Isaksson, Y. Ozaki, Studies on the structure of water using two-dimensional near-infrared correlation spectroscopy and principal component analysis, Anal. Chem. 73 (2001) 3153–3161, https://doi.org/10.1021/ac010102n.
[67] H. Maeda, Y. Ozaki, M. Tanaka, N. Hayashi, T. Kojima, Near Infrared Spectroscopy and Chemometrics Studies of Temperature-Dependent Spectral Variations of Water: Relationship between Spectral Changes and Hydrogen Bonds, J. Near Infrared Spectrosc. 3 (1995) 191–201, https://doi.org/10.1255/jnirs.69.
[68] J. Tukey, Exploratory data analysis, Addison-Wesley, Reading, MA, 1977.
[69] T. Naes, T. Isaksson, T. Fearn, T. Davies, A user Friendly guide to Multivariate Calibration and Classification, NIR Publications, Chichester UK, 2002.
[70] I.A. Cowe, J.W. McNicol, The Use of Principal Components in the Analysis of Near-Infrared Spectra, Appl. Spectrosc. 39 (1985) 257–266, https://doi.org/10.1366/0003702854248944.
[71] P.C. Williams, D.C. Sobering, Attempts at standardization of hardness testing of wheat. II. The near-infrared reflectance method, Cereal Foods World. 31 (1986) 417–420.
[72] M. Lukacs, G. Bazar, B. Pollner, R. Henn, C.G. Kirchler, C.W. Huck, Z. Kovacs, Near infrared spectroscopy as an alternative quick method for simultaneous detection of multiple adulterants in whey protein-based sports supplement, Food Control 94 (2018) 331–340, https://doi.org/10.1016/J.FOODCONT.2018.07.004.
[73] R. Tsenkova, Aquaphotomics: Water in the biological and aqueous world scrutinised with invisible light, Spectrosc. Eur. 22 (2010) 6–10.
[74] R. Tsenkova, J. Munćan, B. Pollner, Z. Kovacs, Essentials of aquaphotomics and its chemometrics approaches, Front. Chem. 6 (2018) 363, https://doi.org/10.3389/fchem.2018.00363.
[75] K. Miyamoto, Y. Kitano, Non-Destructive Determination of Sugar Content in Satsuma Mandarin Fruit by near Infrared Transmittance Spectroscopy, J. Near Infrared Spectrosc. 3 (4) (1995) 227–237.
[76] F. Chauchard, J.M. Roger, V. Bellon-Maurel, Correction of the Temperature Effect on near Infrared Calibration—Application to Soluble Solid Content Prediction, J. Near Infrared Spectrosc. 12 (2004) 199–205, https://doi.org/10.1255/jnirs.427.
[77] S. Kawano, H. Abe, M. Iwamoto, Development of a Calibration Equation with Temperature Compensation for Determining the Brix Value in Intact Peaches, J. Near Infrared Spectrosc. 3 (4) (1995) 211–218.
[78] J.T. Bell, N.A. Krohn, The near-infrared spectra of water and heavy water at temperatures between 25 and 390 [1], J. Phys. Chem. 74 (1970) 4006, https://doi.org/10.1021/j100716a028.
[79] D. Cozzolino, L. Liu, W.U. Cynkar, R.G. Dambergs, L. Janik, C.B. Colby, M. Gishen, Effect of temperature variation on the visible and near infrared spectra of wine and the consequences on the partial least square calibrations developed to measure chemical composition, Anal. Chim. Acta. 588 (2007) 224–230, https://doi.org/10.1016/j.aca.2007.01.079.
[80] W.S. Pegau, J.R.V. Zaneveld, Temperature-dependent absorption of water in the red and near-infrared portions of the spectrum, Limnol. Oceanogr. 38 (1993) 188–192, https://doi.org/10.4319/lo.1993.38.1.0188.
[81] W.S. Pegau, D. Gray, J.R.V. Zaneveld, Absorption and attenuation of visible and near-infrared light in water: dependence on temperature and salinity, Appl. Opt. 36 (1997) 6035, https://doi.org/10.1364/ao.36.006035.
[82] J.J. Workman, L. Weyer, Practical Guide and Spectral Atlas for Interpretive Near-Infrared Spectroscopy, 2nd ed., CRC Press, 2012.
[83] M. Chaplin, Water structure and science, (2019). http://www1.lsbu.ac.uk/water/water_vibrational_spectrum.html (accessed January 29, 2019).
[84] J.M. Sullivan, M.S. Twardowski, J.R.V. Zaneveld, C.M. Moore, A.H. Barnard, P.L. Donaghay, B. Rhoades, Hyperspectral temperature and salt dependencies of absorption by water and heavy water in the 400-750 nm spectral range, Appl. Opt. 45 (21) (2006) 5294.
[85] J. Workman, 14. SW-NIR For Organic Composition Analysis, in: Handb. Org. Compd. NIR, IR, R, UV-Vis Spectra Featur. Polym. Surfactants, 2001. https://doi.org/10.1016/B978-012763560-6/50017-9.
[86] W.H. Robertson, E.G. Diken, E.A. Price, J.-W. Shin, M.A. Johnson, Spectroscopic determination of the OH- solvation shell in the OH-.(H2O)n clusters., Science. 299 (2003) 1367–72. https://doi.org/10.1126/science.1080695.
[87] J.M. Headrick, E.G. Diken, R.S. Walters, N.I. Hammer, R.A. Christie, J. Cui, E.M. Myshakin, M.A. Duncan, M.A. Johnson, K.D. Jordan, Spectral Signatures of Hydrated Proton Vibrations in Water Clusters, Science 308 (5729) (2005) 1765–1769.
[88] D. Wei, D.R. Salahub, Hydrated proton clusters: Ab initio molecular dynamics simulation and simulated annealing, J. Chem. Phys. 106 (1997) 6086–6094, https://doi.org/10.1063/1.468256.
[89] K. Mizuse, A. Fujii, Tuning of the Internal Energy and Isomer Distribution in Small Protonated Water Clusters H + (H 2 O) 4–8: An Application of the Inert Gas Messenger Technique, J. Phys. Chem. A. 116 (2012) 4868–4877, https://doi.org/10.1021/jp302030d.
[90] K. Weber, A. Nielsen, Johnson, Isolating the spectroscopic signature of a hydration shell with the use of clusters: superoxide tetrahydrate, Science 287 (2000) 2461–2463.
[91] J. Workman, Handbook of organic compounds: NIR, IR, Raman, and UV spectra featuring polymers and surfaces, Academic Press, San Diego, USA, 2001.
[92] J.-W. Shin, N.I. Hammer, E.G. Diken, M.A. Johnson, R.S. Walters, T.D. Jaeger, M. A. Duncan, R.A. Christie, K.D. Jordan, Infrared Signature of Structures Associated with the H + (H 2 O) n (n = 6 to 27) Clusters, Science 304 (5674) (2004) 1137–1140.
[93] M.K. Phelan, C.H. Barlow, J.J. Kelly, T.M. Jinguji, J.B. Callis, Measurement of caustic and caustic brine solutions by spectroscopic detection of the hydroxide ion in the near-infrared region, 700–1150 nm, Anal. Chem. 61 (1989) 1419–1424, https://doi.org/10.1021/ac00188a023.
[94] J. Zumba, J. Rodgers, M. Indest, Impact of temperature and relative humidity on the near infrared spectroscopy measurements of cotton fiber micronaire, Text. Res. J. 88 (20) (2018) 2279–2291.
[95] P.E. Ciddor, Refractive index of air: new equations for the visible and near infrared, Appl. Opt. 35 (9) (1996) 1566.
[96] T. Giordanengo, J.P. Charpentier, J.M. Roger, S. Roussel, L. Brancheriau, G. Chaix, Correction of moisture effects on near infrared calibration for the analysis of phenol content in eucalyptus wood extracts , Ann. For. Sci. 65 (2011) 803. https://doi.org/10.1051/forest:2008065ï.
[97] J.G. Davis, K.P. Gierszal, P. Wang, D. Ben-Amotz, Water structural transformation at molecular hydrophobic interfaces, Nature 491 (2012) 582–585, https://doi.org/10.1038/nature11570.
[98] S.S. Xantheas, Theoretical Study of Hydroxide Ion-Water Clusters, J. Am. Chem. Soc. 117 (1995) 10373–10380, https://doi.org/10.1021/ja00146a023.
[99] P. Rhine, D. Williams, G.M. Hale, M.R. Querry, Infrared Optical Constants of Aqueous Solutions of Electrolytes. Acids and Bases, J. Phys. Chem. 78 (14) (1974) 1405–1410.
[100] H.J. Deyerl, A.K. Luong, T.G. Clements, R.E. Continetti, Transition state dynamics of the OH + H2O hydrogen exchange reaction studied by dissociative photodetachment of H3O2–, Faraday Discuss. 147–60 (2000).
[101] A. Heiman, S. Licht, Fundamental baseline variations in aqueous near-infrared analysis, Anal. Chim. Acta. 394 (1999) 135–147, https://doi.org/10.1016/S0003-2670(99)00312-8.

[102] Climate-data.org, Wakayama climate: Average Temperature, weather by month, Wakayama weather averages - Climate-Data.org, (n.d.). https://en.climate-data.org/asia/japan/wakayama-prefecture/wakayama-6178/ (accessed September 27, 2021).
[103] A. Inoue, K. Kojima, Y. Taniguchi, K. Suzuki, Near-infrared spectra of water and aqueous electrolyte solutions at high pressures, J. Solution Chem. 13 (1984) 811–823, https://doi.org/10.1007/BF00647696.
[104] K. Molt, A. Niemöller, Y.J. Cho, Analysis of aqueous solutions by near-infrared spectrometry (NIRS) II. Titrations of weak and very weak acids with strong bases, J. Mol. Struct. 410–411 (1997) 565–572, https://doi.org/10.1016/S0022-2860(96)09706-2.
[105] V.J. Frost, K. Molt, Analysis of aqueous solutions by near-infrared spectrometry (NIRS) III. Binary mixtures of inorganic salts in water, J. Mol. Struct. 410 (1997) 573–579.